Tropical Cloud Feedbacks and Natural Variability of Climate

R. L. MILLER AND A. D. DEL GENIO

NASA Goddard Institute for Space Studies, New York, New York

(Manuscript received 9 September 1992, in final form 27 December 1993)

ABSTRACT

Simulations of natural variability by two GCMs are examined. One GCM is a sector model, allowing relatively rapid integration without simplification of the model physics, which would potentially exclude mechanisms of variability. Two mechanisms are found in which tropical surface temperature and SST vary on interannual and longer timescales. Both are related to changes in cloud cover that modulate SST through the surface radiative flux.

Over the equatorial ocean, SST and surface temperature vary on an interannual timescale, which is determined by the magnitude of the associated cloud cover anomalies. Over the subtropical ocean, variations in low cloud cover drive SST variations. In the sector model, the variability has no preferred timescale, but instead is characterized by a "red" spectrum with increasing power at longer periods. In the terrestrial GCM, SST variability associated with low cloud anomalies has a decadal timescale and is the dominant form of global temperature variability.

Both GCMs are coupled to a mixed layer ocean model, where dynamical heat transports are prescribed, thus filtering out ENSO and thermohaline circulation variability. The occurrence of variability in the absence of dynamical ocean feedbacks suggests that climatic variability on long timescales can arise from atmospheric processes alone.

1. Introduction

General circulation models (GCMs) predict warming in response to anthropogenic CO_2 and other greenhouse gases (Schlesinger and Mitchell 1987). The warming is global in extent, and scientists have attempted to validate the models by comparison to the globally averaged surface temperature observed during the past century (e.g., Hansen and Lebedeff 1988). The observations show evidence of warming, although the comparison raises the question of how to distinguish the trend due to increased CO_2 from variations that result from other climatic processes.

Large departures from the current climate occurred prior to the Industrial Revolution and the accelerated burning of fossil fuels. The most recent example is the Little Ice Age. Broecker (1992) has argued that its onset was an example of natural variability—that is, a fluctuation caused by processes intrinsic to the climate, rather than by changes in the external forcing such as solar variability. Broecker suggested that natural variability could also account for the warming observed during the first half of this century. Unfortunately, the limited measurement record makes it difficult to distinguish precisely the effects of natural variability upon surface temperature. Observations of fundamental atmospheric quantities such as wind, pressure, moisture, and temperature throughout the troposphere exist, if incompletely, only for the past few decades. Thus, mechanisms of natural variability characterized by longer timescales are not well described in the observations, and one might question whether all mechanisms have even been identified.

To the extent that they are believed to mimic climate accurately and contain the physics responsible for natural variability, GCMs can offer guidance, since they can be integrated to simulate arbitrarily long periods. Oceanographers have found variability in the thermohaline circulation of ocean GCMs with periods of decades, centuries, and millenia (reviewed by Weaver and Hughes 1993). Variability with similar periods has been found in coupled oceanic and atmospheric models (Manabe and Stouffer 1988; Sausen et al. 1988; Mehta 1992).

While the coupling of atmospheric and oceanic models is desirable, insofar as the modes of variability inherent to each can interact, questions remain about the variability of the individual systems. For example, with its faster overturning and smaller heat capacity, it is not obvious whether the atmosphere can contribute to variability on the decadal and longer timescales found in ocean GCMs.

The rate of meridional overturning is not the only timescale intrinsic to climate. For example, Weaver and Sarachik (1991) found decadal fluctuations in their ocean model's deep-water formation, even though

Corresponding author address: R. L. Miller, Department of Applied Physics, Columbia University, 2880 Broadway, New York, NY 10025.

hundreds of years are required by fluid parcels to traverse the entire "conveyor belt." As for the atmosphere, Hasselmann (1976) and, more recently, Wigley and Raper (1990) have argued that climatic variations could be forced by variations on the shorter timescale of weather in the same way that the ensemble-average drift of a random-walk process increases with time. James and James (1989) suggest that this is the source of the decadal variability found in their model. They integrated an atmospheric GCM (albeit with highly simplified parameterizations of radiation and latent heating) and found that a particular spherical harmonic of the temperature field varied with a decadal period. This harmonic averages globally to zero, however, and whether the decadal oscillation is reflected in the global-mean temperature—which is of interest to modelers attempting to validate GCM greenhouse experiments—was unstated. Thus, whether atmospheric processes could lead to variability of the globally averaged temperature on a similar decadal timescale remained unclear.

One might question whether GCMs can be used to identify the entire spectrum of natural variability. This question arises since GCMs, lacking infinite resolution, must parameterize certain physical processes, such as convection or radiation, in terms of variables resolved over relatively coarse grids. To the extent that certain physical processes are simplified or absent, modes of natural variability that result from these processes will be absent in a model. For example, James and James approximated the effects of radiation in their model with Newtonian cooling, implicitly holding constant the cloud cover. Consequently, variability depending upon cloud cover anomalies that alter the radiation budget of the troposphere would be missing from their model.

GCMs forced with increased surface temperatures have demonstrated that cloud cover can feed back and either oppose or enhance the original warming, depending upon the model's parameterization of cloud cover (Cess et al. 1990). In this study, we consider whether cloud cover feedbacks can result in temperature variability in an unforced model.

In section 2, we describe two GCMs used to address this question. One GCM has been transformed into a sector model to allow faster integration, although in neither model have the physical parameterizations of radiation and convection, for example, been simplified to increase the integration speed. We find two cloud feedbacks resulting in variations of surface temperature and SST on interannual and longer timescales, which are described in section 3.

In the first, evaporative anomalies drive variations in equatorial SST. However, the timescale of the variability is set by the magnitude of the cloud cover anomaly, which acts as a negative feedback in response to changing SST.

The second feedback is initially positive: a decrease in subtropical cloud cover enhances the surface heating by solar radiation, increasing the temperature, which further decreases the low cloud cover. Barnett et al. (1992) have analyzed the variability of the global-mean surface temperature calculated from a 100-year simulation of climate using the Goddard Institute for Space Studies (GISS) GCM (Hansen et al. 1988). They find that the surface temperature is largely controlled by surface solar radiation, which in turn is modulated by low cloud cover. In section 4, we argue that variability of the globally averaged surface temperature in this model is largely a result of the second cloud feedback.

In the concluding section, we discuss implications of our model behavior for cloud cover feedbacks in the atmosphere. We also consider the implications for the modeling of natural variability.

2. Model description

We use two GCMs to study cloud cover feedbacks associated with decadal variability in the globally averaged surface temperature. The first is the current version of the GISS GCM [referred to as model II by Hansen et al. (1983)], used to create the 100-year simulation originally described in Hansen et al. (1988). Computational costs prohibited longer integrations with this model, so a sector version was constructed to carry out a 1000-year simulation. That is, atmospheric variables in the second GCM were computed only within a sector covering 120° of longitude. The circulation outside this region was calculated assuming zonal periodicity, thus accounting for the circulation over the remaining two-thirds of the planet. To be consistent with the assumption of a zonally periodic climate, the oceans and continents were relocated from their terrestrial positions, as shown in a map of SST averaged over the last 900 years of the simulation (Fig. 1). The geography was arranged to depart from that of the earth as little as possible—in particular, the ratio of land to ocean at each latitude is identical. The disadvantage of a sector model is that the climate of a planet resembling the earth is simulated, rather than the climate of the earth itself. However, Table 1 shows that the gross features of the circulation computed using the sector and terrestrial models are quite similar.

The sector model is slightly colder, cloudier, and less energetic than the terrestrial GCM (Table 1). Its convection and large-scale eddy transports, on the other hand, are slightly stronger. The sector model's Hadley cell is almost identical to that of model II; its Walker circulation is somewhat weaker. Otherwise, most differences are within the range of model II's year-to-year variability. We therefore consider the sector model to be an acceptable proxy for the terrestrial GCM. The sector model has the advantage of allowing relatively rapid integration without simplification of the model physics, which would potentially filter out the mechanisms of natural variability that we wish to study.

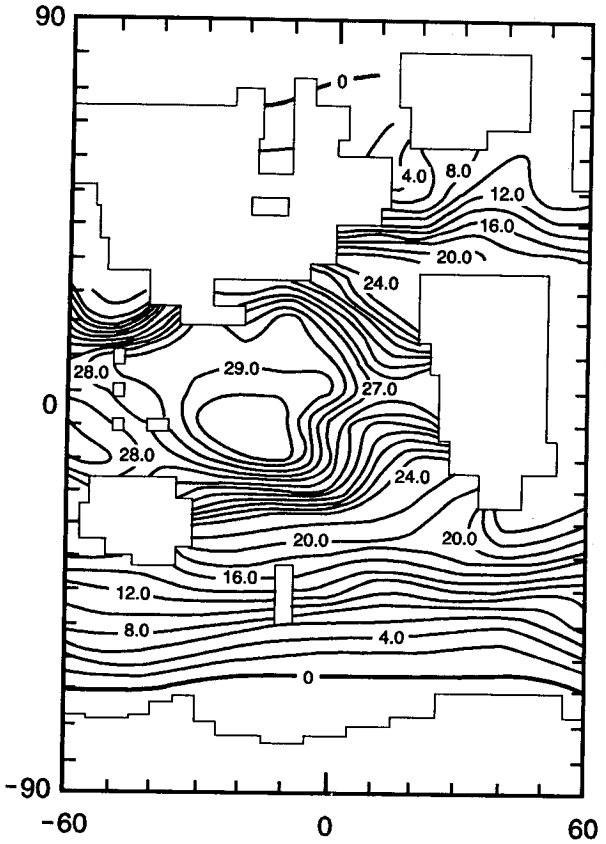

FIG. 1. SST (°C) within the sector model, averaged over the last 900 years of the 1000-year simulation. The contour interval changes from 2.0 to 0.5 above 24°C.

The sector model output was stored as seasonal averages. A seasonal cycle was constructed by averaging each season over the last 900 years of the integration, after the model appeared to have completed its "spinup" (cf. Fig. 2). This cycle was subtracted from the seasonal average to create seasonal anomalies. Unless stated otherwise, all analysis of the sector model in section 3 is carried out using these seasonal anomalies. To analyze the terrestrial GCM in section 4, we used the annual-mean anomalies considered previously by Barnett et al. (1992). That is, we computed an average of each field over the length of the simulation and subtracted it from the annual mean to create an annual-mean anomaly.

Both models have spatial resolution of 8° latitude by 10° longitude and are coupled to a "Q-flux" ocean model (Miller et al. 1983). Heat transport by ocean currents is specified a priori, although the mixed layer temperature is free to vary from year to year as a result of variations of the surface fluxes. The model is forced by solar radiation along with the prescribed ocean transports, both with a specified seasonal cycle.

Since the ocean model is not fully interactive, it is unclear whether the feedbacks and variability described in the next section have counterparts in the actual climate. Although lacking a thermohaline circulation, the model is useful nonetheless in that it filters out variability found in ocean GCMs. Consequently, any variability exhibited by our GCM can be ascribed to processes intrinsic to the atmosphere and is not simply the atmospheric response to oceanic variability.

3. Cloud feedbacks in the sector model

Figure 2 shows the globally averaged surface temperature over the entire 1000-year simulation. The cloud feedbacks associated with temperature variability were found over the tropical oceans, where surface temperature and SST are well correlated (not shown).

TABLE 1. Comparison of annual-mean climate diagnostics from the sector model and GISS model II (i.e., the terrestrial GCM). All quantities are global means unless otherwise indicated.

	Sector model	Terrestrial model
Sea surface temperature (°C)	14.5	15.5
Precipitation (mm day^{-1})	3.3	3.2
TOA energy budget (W m^{-2})		
Absorbed solar	233.8	240.5
Outgoing longwave	−230.9	−233.0
Surface energy budget (W m^{-2})		
Absorbed solar	167.0	173.4
Net longwave	−46.8	−50.0
Latent heat flux	−97.2	−91.8
Sensible heat flux	−28.2	−25.7
Total cloud cover (%)	53.8	51.7
High	29.4	29.3
Middle	21.2	19.5
Low	39.3	35.9
Moist convective heating ($\times 10^{14}$ W)	448.7	431.5
Tropospheric energy ($\times 10^{18}$ J)		
APE	3145.7	3306.6
ZKE	287.3	253.5
EKE	376.1	426.2
Tropospheric energy conversion ($\times 10^{13}$ W)		
APE → EKE	64.8	63.5
EKE → ZKE	−2.6	−5.3
ZKE → APE	−39.2	−36.0
NH poleward eddy transports		
Dry static energy ($\times 10^{14}$ W)	10.6	9.6
Latent heat ($\times 10^{14}$ W)	11.1	10.7
Angular momentum ($\times 10^{18}$ J)	5.5	3.8
Peak zonal wind (m s^{-1}) 31°, 201 mb		
NH	26.3	25.9
SH	33.3	33.5
Peak streamfunction ($\times 10^{9}$ kg s^{-1})		
Hadley cell, NH/SH	−58/91	−65/90
Ferrel cell, NH/SH	2/−13	2/−5
Walker Cell, equatorial mean vertical velocity (mm s^{-1})		
W. Pacific	1.78	2.42
E. Pacific	0.08	−1.35

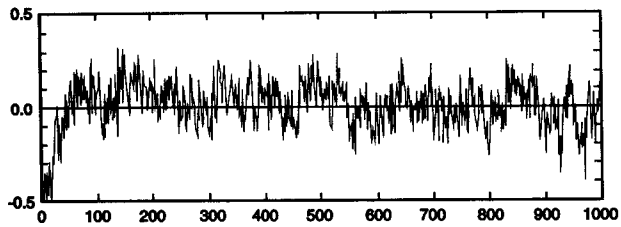

FIG. 2. Anomalies of annually averaged global-mean surface air temperature (°C) during the 1000-year integration of the sector model.

Because SST is easier to diagnose, given our simple ocean model, its variability will be the focus of our analysis.

The standard deviation of seasonal anomalies of SST is shown in Fig. 3. One maximum, denoted by **A**, occurs at equatorial latitudes over the central ocean. Two other regions of large variance, denoted by **B** and **C**, occur in the eastern subtropics of the Northern and Southern Hemisphere, respectively.

The following subsections will describe more fully the variability at these locations, including characteristic timescales, and will suggest a mechanism responsible for the large variations of SST at these locations.

a. The ITCZ oscillation

The correlation of SST at the equatorial location **A** with respect to other locations is shown in Fig. 4a. Large correlations are mainly confined to equatorial latitudes south of the equator. In contrast, Fig. 4b shows that rainfall anomalies associated with those at location **A** extend across the equator, where they are anticorrelated. To understand why rainfall anomalies extend beyond the region of SST variability, we considered the moisture budget. Figure 4c shows that evaporative anomalies associated with location **A** are coincident with those of SST and do not extend across the equator. This implies that precipitation anomalies north of the equator are linked to those at location **A** by dynamical fluxes of water vapor. This is consistent with the correlation map of moist convective cloud cover (Fig. 4d), which implies that a convectively driven circulation links the two centers of the precipitation anomaly.

While the large SST variability centered at location **A** is confined to south of the equator, the convective response occurs in both hemispheres, resulting in a split ITCZ during the years when the mixed layer at location **A** is relatively cold. This is shown in Figs. 5a and 5b. The former shows the total annual-mean precipitation for a year when SST is above normal at location **A**. The model ITCZ appears as a single band slightly south of the equator. Figure 5b corresponds to a year when SST at the same location is anomalously cold. Now rainfall is diminished locally, and the mixed layer is warmer just across the equator to the north (not shown), where convection and rainfall are enhanced. Toward the eastern end of the equatorial warm pool, the ITCZ divides into a double-cell pattern.

The model ITCZ was found to alternate between a single- and double-celled pattern somewhat irregularly, with a period of around 5 years. To estimate a characteristic timescale for the variability more precisely, the spectrum of SST at location **A** was computed (Fig. 6a). The spectral shape is "red"—that is, characterized by increasing power toward low frequencies—with significant departures from redness at periods between 1 and 10 years. These departures will be interpreted from a physical standpoint below.

To determine what causes SST to vary at location **A**, we examined the surface energy balance. Variations in SST are relatively easy to diagnose in a mixed layer ocean model, since the dynamical ocean heat transport is prescribed to be the same from year to year. Consequently, seasonal anomalies of SST can result only from variations in the surface fluxes. Figure 7a shows the covariance of various terms in the surface energy budget with respect to seasonal anomalies of SST. Warming results from the latent heat flux anomalies, as indicated by positive covariance at negative lags. Warming of the mixed layer is followed within a season by enhanced convection and rainfall (Fig. 7b). This convection has two effects. As a result of the compensating subsidence noted above, rainfall patterns are altered beyond the range of the original SST anomaly. Second, the cloud cover associated with enhanced rainfall reflects sunlight (Fig. 7c), shielding the surface from solar radiation and acting to cool the original SST anomaly (Fig. 7a).

Next we consider whether the evaporative forcing that drives variations in SST is in turn dependent upon SST. More generally, we ask whether the variations at location **A** correspond to an evaporative "normal mode" of the model, or whether evaporation is largely independent of the underlying SST, so that the temperature variability is driven externally by "noise." One means to distinguish between these two possibilities is

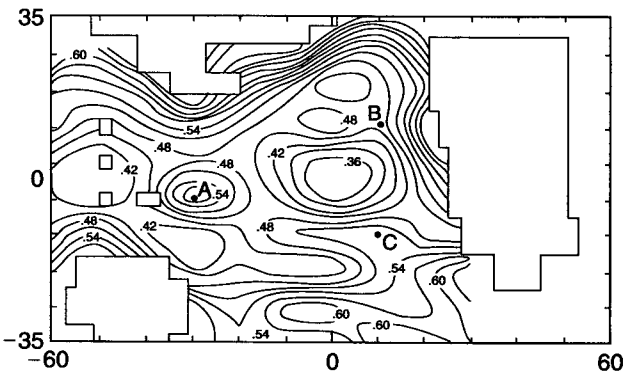

FIG. 3. Standard deviation (°C^2) of sector model seasonal anomalies of tropical SST. Here **A**, **B**, and **C** mark grid points whose variability is analyzed in the text.

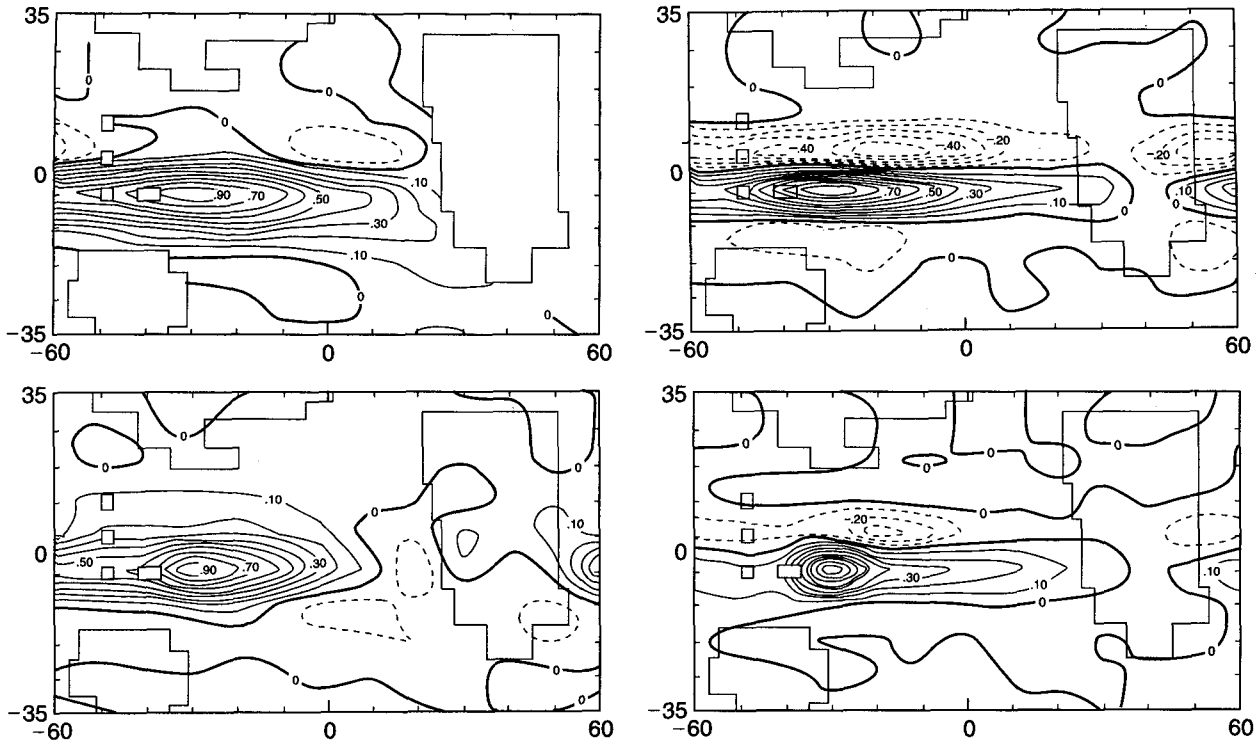

FIG. 4. (a) Correlation between SST at location **A** with SST at other grid points. (b) Same but for precipitation, (c) evaporation, and (d) moist convective cloud cover.

to consider the spectrum of the forcing and response—that is, the latent heat flux and the SST, respectively. At each ocean grid box, the seasonal anomaly of the mixed layer temperature T roughly satisfies

$$c\partial_t T = -\lambda T + \mathcal{E}, \qquad (1)$$

where c is the heat capacity of the mixed layer, $-\lambda T$ is a crude representation of the negative feedback in Fig. 7a resulting from radiation and sensible heating, and $\mathcal{E}$ is the evaporative forcing.

If $\mathcal{E}$ depends upon T, then $\mathcal{E}$ can be linearized and (1) becomes a dispersion relation yielding a preferred timescale for the variability. This timescale would correspond to a peak in the spectra of both SST and evaporation. Alternatively, if $\mathcal{E}$ is unrelated to the underlying SST, then (1) results in a spectrum of SST which is "red," with spectral amplitude smoothly increasing toward longer periods (e.g., Jenkins and Watts 1968, section 6.2.5).

Figure 6a shows the spectrum of SST at location **A**. This spectrum is the average of spectra constructed from successive 100-year intervals offset every 50 years. Averaging increases the prominence of spectral peaks corresponding to periodic phenomena in the model, compared to peaks arising spuriously from the finite length of the time series (e.g., Press et al. 1992, section 13.4). As a null hypothesis, we assume that the evaporative forcing is independent of temperature so that the spectrum, according to (1), is red. This is the bottom dashed line in Fig. 6a. If the variability can be described as a red-noise process, then the entire spectrum will lie below the upper dotted line 95% of the time.

Figure 6a shows that the red spectrum is exceeded by a broad range of frequencies between 1 and 10 years with several estimates above the 95% threshold. Presumably, if evaporation coupled to SST corresponds to a normal mode of the model, then the same broad departure from a red spectrum would be found in the spectrum of the latent heat flux. However, Fig. 6b shows that this is not the case. The evaporative spectrum is nearly flat or "white," with no statistically significant departures at interannual timescales.

It might be argued that the presence of a corresponding timescale in the evaporative spectrum is obscured by other forms of variability at location **A**. In an effort to isolate the ITCZ oscillation, we decomposed the data using the singular value decomposition (SVD) technique described by Bretherton et al. (1992). In this case, our covariance matrix was constructed using evaporation at all tropical stations along with SST lagged by one season. The gravest mode (i.e., the pattern whose covariance matrix most resembles the covariance matrix of the data) for SST has a spatial dependence almost identical to the correlation map of SST in Fig. 4a. The latent heat flux one season earlier

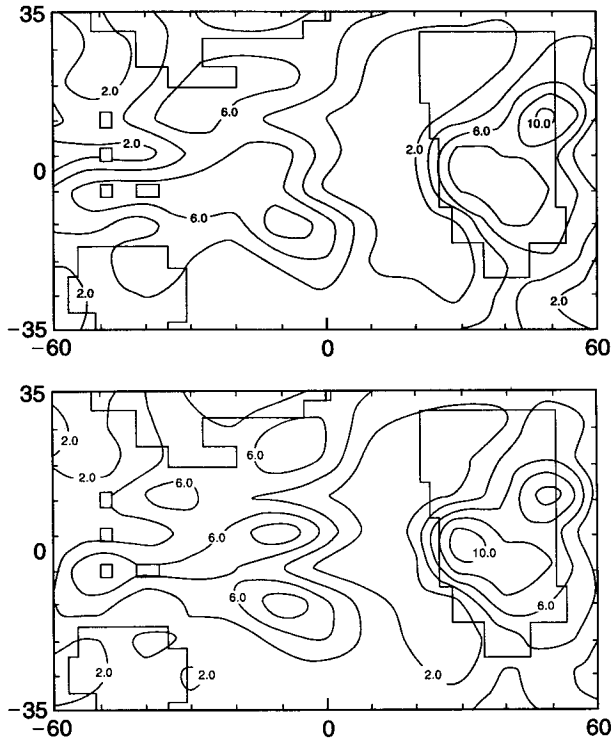

FIG. 5. Annual-mean rainfall (mm day^{-1}) for (a) year 631 and (b) year 599.

has an equally strong resemblance to Fig. 4c. We repeated the spectral analysis, this time with the time series corresponding to each spatial pattern, and found the same result as described above: the SST spectrum was "red" in shape with broad departures at periods between 1 and 10 years. In contrast, the evaporative spectrum was flat, or "white," without significant peaks at corresponding interannual timescales.

The lack of corresponding peaks suggests that the forcing is independent of SST. SST variations at location **A** may still correspond to a normal mode of model variability. However, latent heat fluxes cannot be intrinsic to this mode and can act only as external forcing. Miller and Del Genio (1994) considers a one-dimensional model for mixed layer temperature identical to (1) but with a negative feedback of the form $-\lambda_1 T(t) - \lambda_2 T(t-\tau)$. The first term represents cooling by net longwave radiation which, according to the Stefan–Boltzmann expression, largely depends upon the instantaneous temperature. The negative feedback due to solar radiation is expressed in the second term, which is lagged with respect to temperature, since convective cloud cover does not adjust immediately to changes in SST but requires a season or so (Fig. 7b). As a result of this adjustment time τ, nearly neutral oscillatory solutions are possible, and given external forcing (e.g., by evaporation) to continually reexcite the solution against longwave damping, these solutions can result in a broad spectral peak centered around a period on the order of a few years. This timescale, the dominant timescale of SST variability at location **A**, depends upon the adjustment time between SST and convection, along with the strength of the cloud cover feedback upon the surface radiative flux.

Finally, we consider whether the model variability might extend to the terrestrial atmosphere. An obvious limitation of our model is that the ocean cannot respond dynamically to anomalies of SST. This is an especially unrealistic constraint in the vicinity of the equatorial waveguide, where SST is poorly predicted by surface fluxes (Liu and Gautier 1990). Outside this region, the same study found that SST is a strong function of the surface fluxes. Presumably, our model variability could have a terrestrial counterpart in regions where SST is determined mainly by variations in the surface fluxes. These regions must be close enough to warm equatorial SSTs so that convection can occur in response to changes in SST, altering the surface solar flux through changes in the deep convective cloud cover.

Our model has other limitations as well, one being that the negative feedback of solar radiation induced by cloud cover is unrealistically small. This is for two

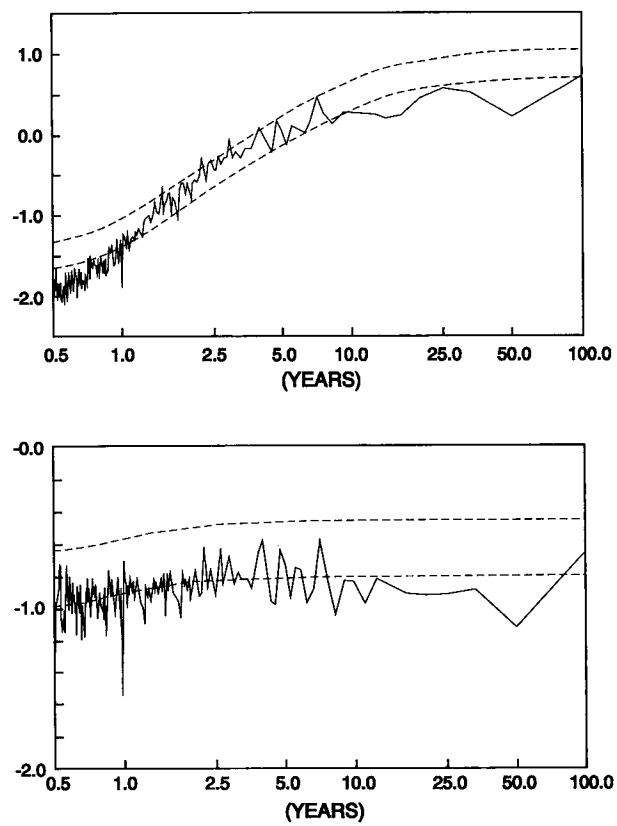

FIG. 6. (a) Logarithm (base 10) of the spectrum of SST at location **A**, constructed by averaging spectra computed for successive 100-year intervals offset every 50 years. (b) Same but for evaporation.

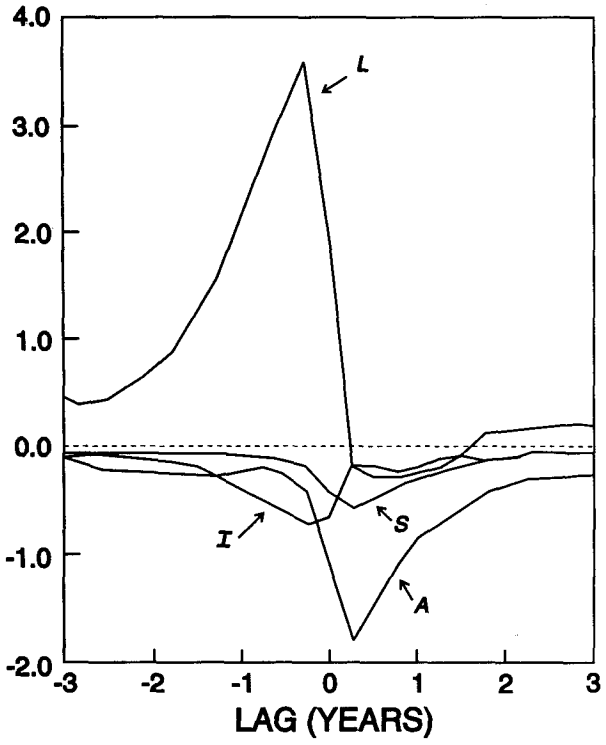

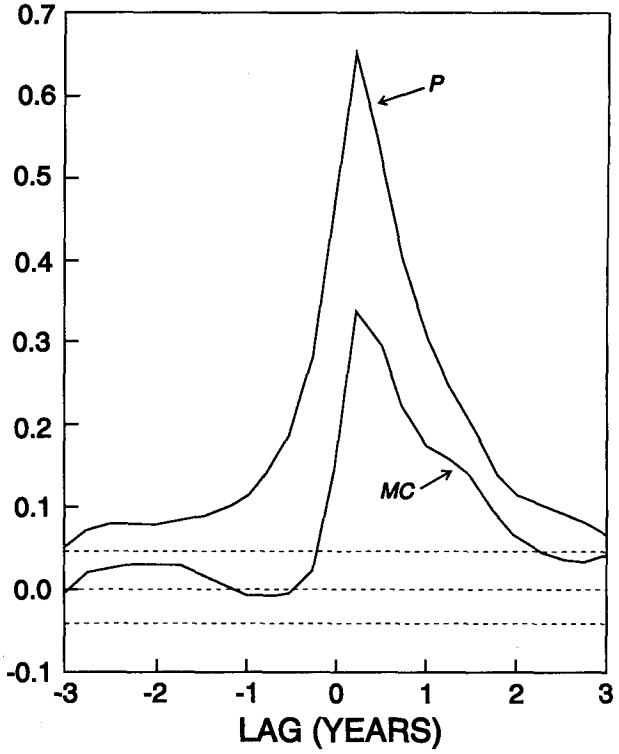

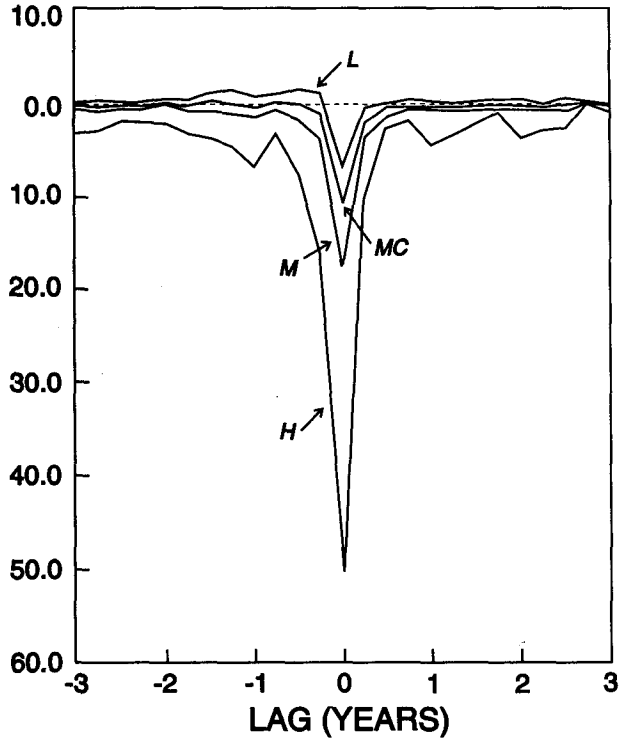

FIG. 7. Lagged covariance and correlations at location **A**. (a) Covariance of SST with surface energy fluxes: absorbed solar (A) and infrared radiation (I), along with latent (L) and sensible (S) heating. (b) Correlation of SST with rainfall (P) and moist convective cloud cover (MC). (c) Covariance of surface-absorbed solar radiation with high (H), middle (M), low (L), and moist convective (MC) cloud cover.

reasons. One is that high clouds are unrealistically transparent in the GISS model, so that surface variability is almost entirely unaffected by high cloud anomalies. Consequently, although the variance of cloud cover at location **A** is largest with respect to high clouds (Fig. 7c), shielding of the surface from sunlight

is almost entirely a result of the optically thicker mid-level clouds. Note also that low clouds increase only slightly with SST (Figs. 7a and 7c). In part, this is a result of damping of relative humidity increases in convecting regions by parameterized cumulus subsidence. We will describe in the following subsection how a feature of the GISS cloud cover parameterization unrelated to relative humidity can artificially inhibit the formation of low clouds. In the absence of significant perturbations to the total cloud optical thickness by high and low clouds, the negative feedback to SST anomalies is underestimated by the model. In addition, cloud cover feedbacks upon the surface energy budget depend almost entirely upon the presence of substantial middle cloud variability. We will return to this point in section 4.

b. The low cloudiness feedback

Away from the equator, tropical SST variability is largest in the eastern subtropics, and at locations **B** and **C** in particular. Since the mechanisms responsible for variability are the same at both locations, only the analysis for location **B** will be presented.

Figure 8 shows the correlation of SST at location **B** with other locations. The variability is largely confined to the eastern subtropics in the Northern Hemisphere. Spectral analysis of SST at location **B** gives a "red" spectrum with no significant departures (not shown). That is, variability increases smoothly toward longer periods, in contrast to the equatorial location **A**, where the variability has a dominant timescale of a few years. However, we will show in section 4 that the same mechanism operating at location **B** results in a strong decadal signal in the terrestrial model.

The covariance of SST with respect to the surface energy fluxes is shown in Fig. 9a. In contrast to the equatorial variability at location **A**, variations of SST in the eastern subtropics are primarily driven by anomalies in solar radiation, whereas latent heat fluxes provide a strong negative feedback. Figure 9b shows the covariance of solar radiation absorbed at the surface

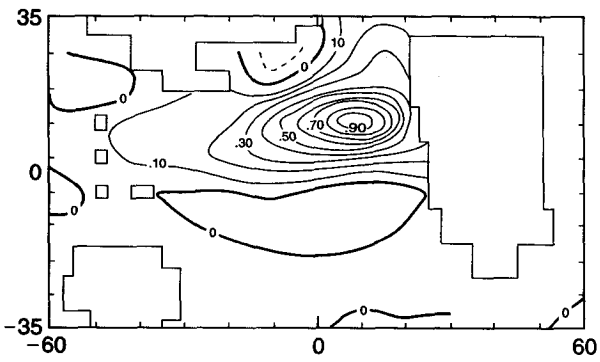

FIG. 8. Correlation between SST at location **B** with SST at other locations.

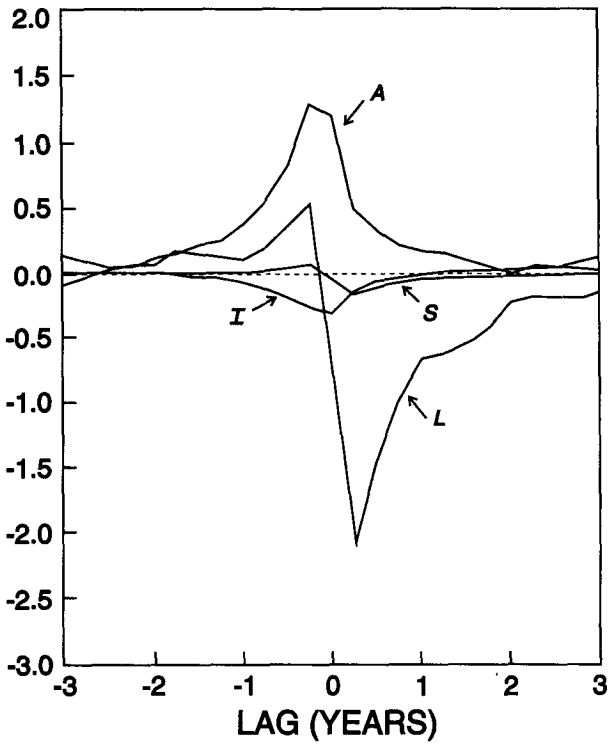

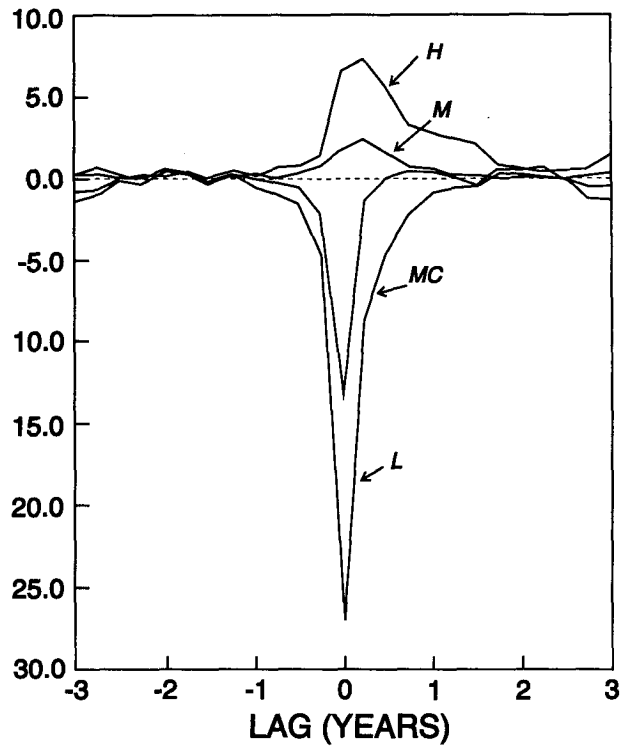

FIG. 9. Lagged covariance at location **B**. (a) Covariance of SST with surface energy fluxes: absorbed solar (A) and infrared radiation (I), along with latent (L) and sensible (S) heating. (b) Covariance of surface-absorbed solar radiation with high (H), middle (M), low (L), and moist convective (MC) cloud cover.

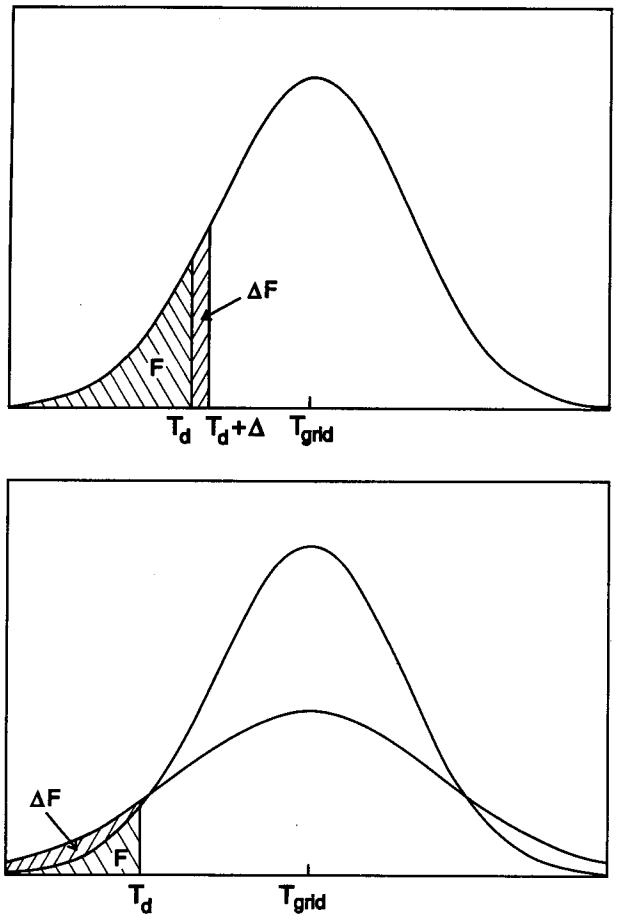

FIG. 10. A schematic description of the cloud fractional area parameterization in the GISS GCM. Cloud cover increases either (a) because the dewpoint increases, or (b) because the variance of the subgrid-scale temperature increases. Here T_{grid} is the resolved temperature of the grid box, T_d is the dewpoint calculated from the resolved temperature and humidity, and F is the fractional saturation of the grid box.

with respect to cloud cover at various levels in the model. The strongest covariance is with respect to low clouds. Since low clouds have the greatest optical thickness, their effect upon surface solar fluxes is even stronger, compared to clouds at other heights, than indicated by the figure.

Warming at location **B** is associated with a decrease of low cloud cover that increases the solar radiation absorbed by the mixed layer. In response to rising SST, low cloud cover initially continues to decrease, rendering a positive feedback (note the positive covariance between SST and solar radiation at positive lags). This behavior contrasts with that of the ITCZ oscillation, wherein cloudiness increases in response to the warming of the boundary layer, reducing sunlight and acting to damp the original SST anomaly.

Before considering whether a positive feedback could result from subtropical low clouds in the real atmosphere, we examine why rising SST causes low clouds to decrease in the model. Cloud cover at each grid box is determined by the fraction of air within the box that is saturated. Fractional saturation can occur in the GISS model because temperature is assumed to vary within the grid box with a Gaussian distribution about the resolved temperature. To compute the fractional saturation, the percentage of the subgrid-scale temperature falling beneath the dewpoint is calculated. This percentage gives the fractional saturation and thus the cloud cover within the grid box.

As a consequence, cloudiness can decrease in the GISS model from two effects. First, changes in the rates of evaporation or dynamical moisture convergence can decrease the relative humidity and dewpoint. Alternatively, the variance of the subgrid-scale temperature (i.e., the "width" of the Gaussian) can decrease so that a smaller fraction of the grid falls beneath the dewpoint. These two effects are illustrated schematically in Fig. 10.

It would be useful to determine which of the two parameters, relative humidity or the subgrid-scale temperature variance, has the greatest influence upon subtropical low cloudiness at location **B**. However, diagnosing the relation between relative humidity and low cloud cover is difficult for two reasons. First, the model provides only seasonal averages of relative humidity and cloud cover, so that the two quantities may appear only slightly related to each other, despite the explicit (albeit nonlinear) relation between them at each model time step. Another problem is that while seasonally averaged cloud cover is archived at each grid box, only zonal means of relative humidity are available.

We have made two calculations in an effort to deduce, despite these uncertainties, what determines low cloudiness, and both suggest the same conclusion. First, we correlated the zonally averaged values of relative humidity and the subgrid-scale variance with the zonally averaged cloudiness. The results are shown in Table 2. Second, we correlated at each point the low cloudiness with respect to subgrid-scale temperature variance, along with the relative humidity constructed from the seasonally averaged humidity and temperatures in the model layers corresponding to low clouds.

Both calculations suggest that as SST rises over location **B** (as well as **C**), so does the low-level relative

TABLE 2. Correlations of zonally averaged SST, low cloudiness, relative humidity, and the subgrid-scale temperature variance at 12°N in the sector model. (Relative humidity and the subgrid variance are averaged over the model levels corresponding to low clouds.)

	SST	Low clouds	RH	T var.
SST	1.00			
Low cloudiness	−0.52	1.00		
RH	0.26	−0.23	1.00	
Subgrid t var.	−0.22	0.71	−0.13	1.00

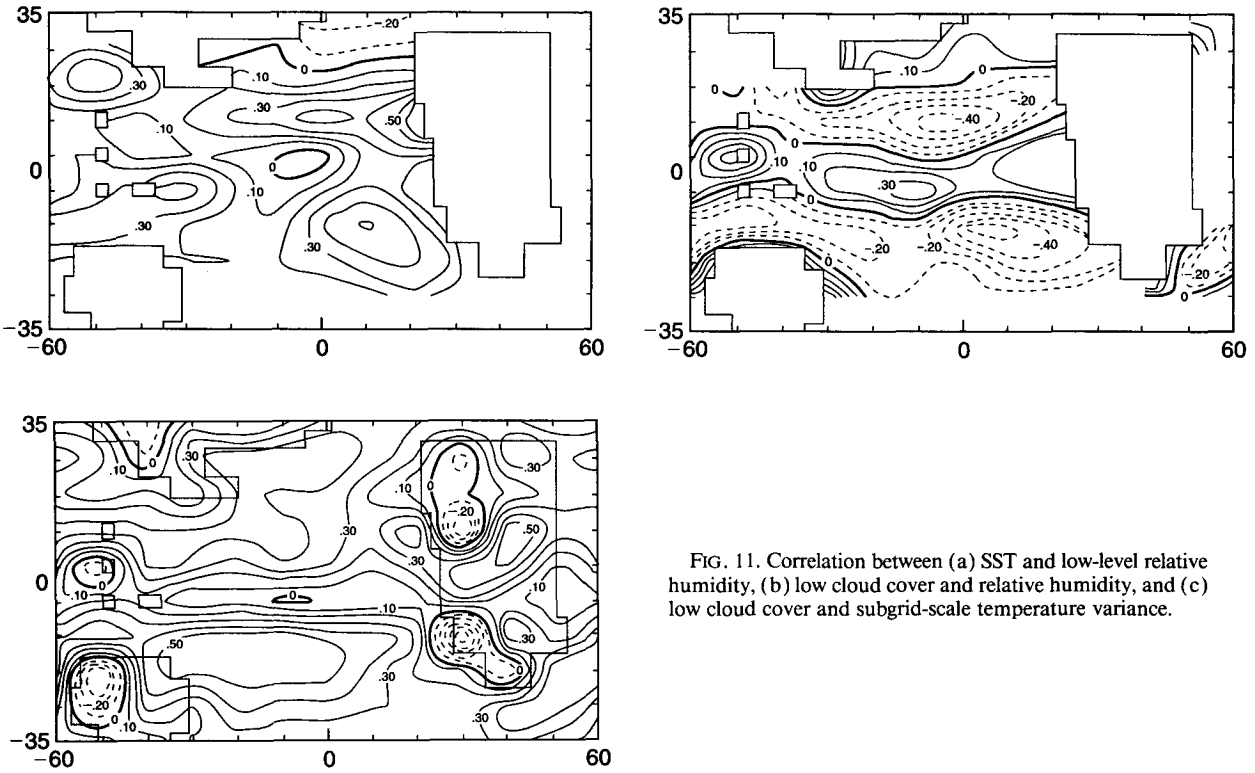

FIG. 11. Correlation between (a) SST and low-level relative humidity, (b) low cloud cover and relative humidity, and (c) low cloud cover and subgrid-scale temperature variance.

humidity (Fig. 11a). This would lead to an increase in low cloud cover, the opposite of what occurs (Fig. 11b). As a consequence, the decrease in low cloudiness associated with rising temperature must result from reduced subgrid-scale temperature variance, or equivalently, from a "narrowed Gaussian." This is demonstrated by Fig. 11c.

This leads us to consider what causes the subgrid-scale variance to decrease, resulting in reduced cloud cover and a positive feedback, rather than the increased cloud shielding that characterizes the ITCZ oscillation. In the GISS model, the subgrid-scale temperature variance is determined by Fourier analysis of the variance of resolved temperature along the latitude circle of the grid box. Then a least-squares fit to the slope of the spectrum between zonal wavenumbers 7 and 18 (the Nyquist wavenumber) is extrapolated to subgrid scales and the total subgrid-scale variance is estimated, thus determining the "width" of the Gaussian (cf. Eqs. 14–18 of Hansen et al. 1983). The relationship between the resolved temperature and the derived subgrid-scale variance probably defies simple characterization. It seems that a relative increase in variability at large scales, however, is one means of reducing the subgrid variance. For example, warming of relatively cold longitudes generally causes the subgrid variance to decrease. Thus, by warming the eastern tropical ocean, which like its terrestrial counterparts is relatively cold, the temperature gradient is reduced, resulting in a spectral shift toward lower wavenumbers. Consequently, the subgrid-scale variance is reduced so that the Gaussian is "narrowed," and a smaller fraction of the Gaussian distribution falls beneath the dewpoint. As such, cloud cover decreases, assuming that the dewpoint depression is held constant. Presumably, in the GISS model, where the dewpoint depression decreases with increasing SST, the subgrid variance decreases more rapidly, resulting in fewer clouds. Eventually, this positive feedback is arrested since the Gaussian can become only so narrow, whereupon its effect is overtaken by that of the increasing dewpoint.

Among the criticisms of the GISS model II cloud cover parameterization is that the subgrid variance is calculated by extrapolating to larger scales measured only in the longitudinal direction. Consequently, it might be questioned whether a positive feedback could be reproduced in the real atmosphere. This leads us to consider what determines terrestrial subtropical low cloud cover. Slingo (1980) found that such clouds are poorly correlated with boundary layer relative humidity, but instead depend upon the presence of a strong trade inversion. The relation between low cloud cover and the inversion is presumably a consequence of cloud-top entrainment instability (CTEI), wherein clouds are dissipated by turbulence if the cloud-top inversion is sufficiently weak (Randall 1980; Deardorff 1980). A positive feedback can thus occur if the thermodynamic prop-

erties of the subsiding air or the rate of subsidence cause weakening of the inversion. Since the subsiding air originates as outflow from deep convection, whose occurrence reflects the surface conditions over a broad region, the existence of a positive feedback will depend upon how temperature changes over the entire extent of the convective circulation, and not just beneath the region of low clouds.

This geographic coupling is similar to the mechanism by which the positive feedback occurs in the sector model, where the region of variability must be cold relative to other longitudes so that the subgrid-scale variance of temperature is decreased. If a more realistic parameterization of subtropical low cloud cover is found to result in a positive feedback, then it would suggest that the subgrid-scale variance in the present model, which couples temperatures along a latitude circle, is mimicking (fortuitously) the role of air subsiding through the trade inversion by acting as a nonlocal determinant of cloud cover.

4. Cloud feedbacks in the terrestrial model

The GISS model II GCM was integrated to simulate 100 years of terrestrial variability (Hansen et al. 1988). The global-mean surface temperature was found by Barnett et al. (1992) largely to reflect variations in tropical temperature, particularly in the central and east Pacific (cf. their Fig. 3). Barnett et al. argued that variations in tropical surface temperature were driven by anomalous solar radiation absorbed by the mixed layer. Surface solar radiation was in turn controlled by low cloud cover.

To illustrate this relationship, empirical orthogonal functions (EOFs) were computed for the annually averaged anomalies of surface temperature, surface solar radiation, and low cloud cover. The mode accounting for the most variance in each field is shown in Fig. 12. The EOFs for all three fields have their largest amplitudes in the same location, implying that the three fields are physically related, as suggested by Barnett et al. (The correlation of the time series corresponding to the first EOF of surface temperature and low cloud cover is -0.73, while the correlation corresponding to surface temperature and surface solar radiation is 0.54.) Figure 12d shows the globally averaged surface temperature along with the time series of the first surface temperature EOF. Even though the EOF is derived only from tropical stations, the correspondence between the two time series is very close (with a correlation is 0.88), consistent with Barnett et al.'s claim that global variability during the simulation is driven largely by variations in the tropical central and east Pacific. Curiously, warming occurs, along with the associated increase in solar radiation and decrease in low cloudiness, not only in the central and east Pacific, but in the east Atlantic as well. While we might be first inclined to dismiss this correlation between the warming in the two oceans as an artifact of the EOF analysis, we will describe below why such a correlation can occur naturally in the model.

As in the sector model, we are led to consider what causes variations in the low cloudiness, which control surface solar radiation and ultimately SST. Barnett et al. suggested that variations in subsidence control low cloud cover. For example, as rainfall increases in response to rising SST (not shown), so does the anomalous subsidence that would tend to dry out the boundary layer, leading to the observed reduction in cloud cover. The problem with this hypothesis is that as in the sector model, low-level relative humidity in model II is positively correlated with surface temperature (Fig. 13a). That is, relative humidity in the boundary layer increases over warmer waters, despite the increased subsidence resulting from anomalous convection. Furthermore, relative humidity and low cloud cover are *anti*correlated in the region of temperature variability (Fig. 13b).

The other parameter determining cloud cover in the model is the subgrid-scale temperature variance. As in the sector model, the correlation between subgrid-scale variance and low cloudiness is positive (Fig. 13c): low cloud cover decreases because the Gaussian distribution of subgrid-scale temperature "narrows." Presumably, this "narrowing" occurs because warming over the relatively cold central and east Pacific causes a shift in the wavenumber spectrum of the temperature variance at that latitude toward larger scales and lower wavenumbers. In any case, a positive feedback results: increasing temperature reduces the low cloud cover through the subgrid variance, resulting in a greater fraction of solar radiation reaching the surface, further increasing the temperature.

The dependence of low cloudiness upon the subgrid variance also explains why temperature should rise in the east Atlantic in concert with warming in the east and central Pacific. Since the subgrid variance is parameterized to be the same around the entire latitude circle, its decrease will act to reduce low cloud cover at *all* longitudes. Furthermore, the associated increase in east Atlantic surface temperature will reinforce the original decrease of the subgrid variance. This is because the east Atlantic is also cold with respect to the longitudinal average, so that the effect of the warming is again to cause a shift in the temperature spectrum toward lower wavenumbers. Because longitudinal temperature gradients in the Indian Ocean are relatively small, warming in this ocean basin cannot further reduce the subgrid variance: presumably this is why this ocean contributes negligibly to the first surface temperature EOF, in comparison to the east Pacific and Atlantic.

In the sector and terrestrial models, a significant longitudinal temperature gradient is required for this feedback to operate. Otherwise changes in the subgrid

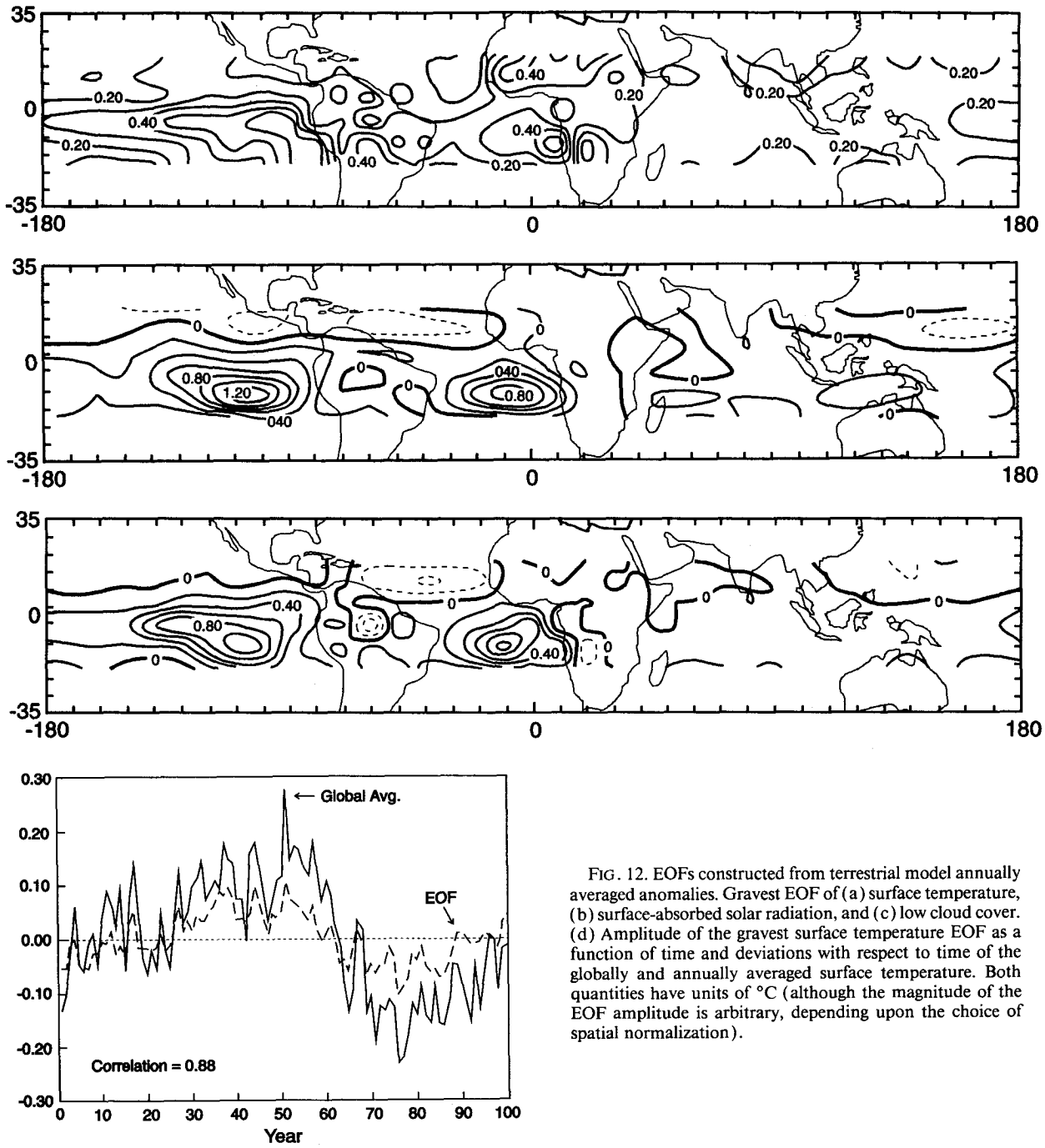

FIG. 12. EOFs constructed from terrestrial model annually averaged anomalies. Gravest EOF of (a) surface temperature, (b) surface-absorbed solar radiation, and (c) low cloud cover. (d) Amplitude of the gravest surface temperature EOF as a function of time and deviations with respect to time of the globally and annually averaged surface temperature. Both quantities have units of °C (although the magnitude of the EOF amplitude is arbitrary, depending upon the choice of spatial normalization).

variance are too small to significantly alter cloudiness. This feedback does not occur in the extratropics or near the equator in the sector model or just north of the equator in model II, where the mean longitudinal gradients of SST are the weakest.

The decadal timescale of the low cloud feedback can be inferred from the time dependence of the gravest surface temperature EOF (Fig. 12d). Its erratic nature is perhaps the result of other modes of atmospheric variability, which can change the subgrid variance through the surface temperature and thus interact with the east Pacific and Atlantic mode described above. This could cause warming trends to become cooling trends and vice versa, although it is difficult to be certain given the complicated dependence of the subgrid variance upon the

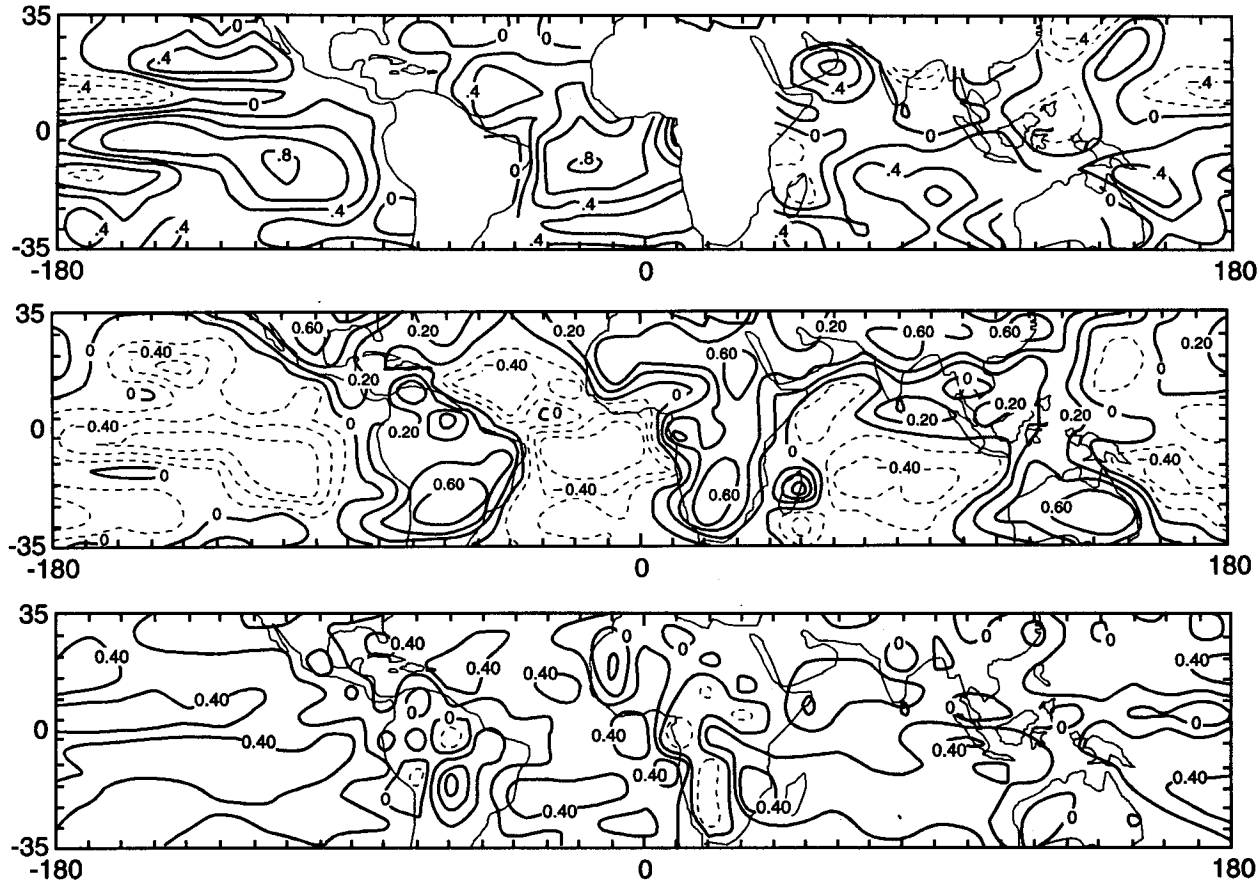

FIG. 13. Correlation between (a) SST and low-level relative humidity, (b) low cloud and relative humidity, and (c) low cloud and subgrid-scale temperature variance in model II.

temperature. Temperature trends can also reverse if the subgrid variance becomes so small that further reduction is not large enough to reduce the fractional saturation in the face of increasing relative humidity.

In summary, the feedback relating low cloud cover, surface solar radiation, and surface temperature was found in both the sector and terrestrial models. It is unclear why the ITCZ oscillation was found only in the former. One difference concerning model behavior involves the amplitude of midlevel cloud anomalies. While a maximum in middle cloud cover variance coincides with the ITCZ in the sector model, the tropical variance of middle clouds is small in model II (e.g., see Figs. 6 and 8 from Barnett et al.). At middle levels, cloud cover is largely a function of relative humidity, since longitudinal gradients of temperature along with variations in the subgrid-scale variance are relatively small. Apparently, more water is converging at midlevels in the sector model. This suggests that the natural variability of a climate model, so far as it is affected by cloud feedbacks, will depend upon the model's convective parameterization, and in particular upon how the parameterization redistributes moisture converged near the surface throughout the depth of the atmosphere.

5. Conclusions

We have considered whether cloud cover feedbacks can lead to climatic variability on interannual and longer timescales. Lacking an observing record of sufficient length, we have turned to GCM simulations. Simulation of climatic timescales is computationally expensive. While integration speed can be increased by simplifying or eliminating model physics, this may lead to the elimination of potential mechanisms of variability. Instead, we have retained the full model physics in a 1000-year simulation, but have increased the integration speed by solving for the climate within only a limited range of longitude.

One question naturally addressed by the 1000-year simulation is whether there exist long timescale mechanisms of variability that have been overlooked in either the comparably brief observational record or previous GCM simulations. Substantial variability at centennial periods is exhibited by the sector model (e.g.,

Fig. 6a). However, this does not necessarily indicate the presence of a hereto undiscovered mechanism operating at this timescale. As a counterexample, Hasselmann (1976) has described how comparatively large variability at long periods (i.e., a "red" spectrum) could be forced by variability on the short day-to-day timescale associated with weather. Consequently, the centennial variability in Fig. 6a, which is not statistically distinct from a "red" spectrum, is possibly forced by processes with shorter timescales. Of the two modes described in section 3, which dominate tropical SST variability, statistically significant departures from a red spectrum occur only in the case of the ITCZ oscillation at interannual periods. This suggests that the physical processes represented by the GCM may be sufficiently resolved in simulations shorter than the 1000 years considered here and that no new behavior will emerge by considering simulations of longer duration. Of course, departures from a "red" spectrum at long periods could potentially occur in long integrations were the model to include a dynamical ocean, such as is lacking in the present model.

Cloud cover feedbacks are fundamental to both modes of tropical surface temperature and SST variability. In the equatorial ocean, latent heat flux anomalies drive temperature variations in the mixed layer. Convection occurs in response to rising SST, enhancing the cloud cover and shielding the ocean surface from solar radiation. The reduced radiative heating of the mixed layer acts as a negative feedback. Variations in equatorial SST are associated with the quasi-regular extension of the model ITCZ into both hemispheres, with a dominant timescale of a few years identified using spectral analysis. A simple mixed layer model (Miller and Del Genio 1994) suggests that the interannual timescale of variability depends upon the strength of the cloud feedback.

Terrestrial counterparts to the model variability could in principle exist where SST is controlled by surface fluxes (i.e., outside the equatorial waveguide) and where the mixed layer is warm enough so that SST anomalies can result in substantial convection and cloud cover feedbacks. Our model behavior also suggests that regular changes in the position of the ITCZ could result not only from dynamical mechanisms (e.g., Hess et al. 1993) but from surface flux anomalies as well.

Over colder subtropical waters, a positive cloud feedback was identified. The effect of clouds upon SST variability in this case is to act as a driving force. A reduction of low cloud cover increases the sunlight incident on the ocean surface, leading to rising SST and a further decrease in cloudiness. This positive feedback occurs because cloud cover in the GISS model is a function not only of the local relative humidity, but also of the temperature at remote grid points. The precise means of coupling in the model is difficult to justify on physical grounds. Nonetheless, Betts (1985) has argued that observed subtropical low clouds are a mixture of boundary layer air and air subsiding through the trade inversion. As a consequence, low cloud cover can decrease despite increasing boundary layer humidity, depending upon the thermodynamic properties of the subsiding air that originates in distant convective centers. Whether a positive feedback could occur through this mechanism remains to be seen.

We note that the sign of cloud feedbacks is not agreed upon in GCM intercomparison experiments (Cess et al. 1990). In addition, a realistic parameterization of subtropical low cloud cover is so far elusive, since a consensus on the physics of CTEI does not yet exist (e.g., MacVean and Mason 1990; Siems et al. 1990). Nonetheless, the models' subtropical variability suggests that *if* a positive cloud feedback is found to occur in the atmosphere, then substantial variability of temperature on interannual and longer timescales can be expected.

This study has implications for simulations of natural variability. First, the existence of cloud feedbacks in a model is strongly dependent upon how moisture converged at low levels is redistributed above by convection. While this conclusion appears self-evident, the absence of the ITCZ oscillation in model II—despite a cumulus parameterization scheme identical to that of the sector model—emphasizes the sensitivity of the model behavior to the moisture redistribution. Second, the presence of cloud feedbacks also depends upon the prescription of optical thickness. In contrast to real tropical high clouds, GISS GCM high clouds barely augment the shielding of the ocean surface by lower-level clouds so that the ITCZ oscillation is absent in model II—despite comparable high cloud variance between the two models.

One goal of natural variability studies might be to measure the magnitude of such variability. For example, one might estimate the variance of the earth's annually averaged surface temperature using a long GCM simulation. Our results suggest that such an experiment be treated with caution. We find that the first EOF of surface temperature in the 100-year terrestrial simulation (Fig. 12a) is related to a parameterization of cloud cover whose physical basis is open to question. This EOF has a correlation of 0.88 with the globally averaged surface temperature, and Barnett et al. (1992) find that it is the dominant mode of global temperature variability (cf. their Figure 3). One might wonder whether the variance of the model surface temperature could change dramatically were the cloud cover determined using a different parameterization.

This example points out that the physics responsible for model variability must be identified before the model can be used to estimate climatic variability. This means that the variability within models must be known to be physically based. In addition, we must be sufficiently familiar with actual modes of climate vari-

ability to be confident that all modes are included in the models.

Acknowledgments. We thank Inez Fung, Syukuro Manabe, David Neelin, and an anonymous reviewer for their comments. This work was supported by the NASA Earth Observing System Interdisciplinary Investigation at GISS and the NASA Tropical Rainfall Measuring Mission.

REFERENCES

Barnett, T. P., A. D. Del Genio, and R. Ruedy, 1992: Unforced decadal fluctuations in a coupled model of the atmosphere and ocean mixed layer. *J. Geophys. Res.*, **97,** 7341–7354.

Betts, A. K., 1985: Mixing line analysis of clouds and cloudy boundary layers. *J. Atmos. Sci.*, **42,** 2751–2763.

Bretherton, C. S., C. Smith, and J. M. Wallace, 1992: An intercomparison of methods for finding coupled patterns in climate data. *J. Climate,* **5,** 541–560.

Broecker, W. S., 1992: Global warming on trial. *Natl. Hist.,* 6–14.

Cess, R. D., and coauthors, 1990: Intercomparison and interpretation of climate feedback processes in 19 atmospheric general circulation models. *J. Geophys. Res.*, **95,** 16 601–16 615.

Deardorff, J. W., 1980: Cloud top entrainment instability. *J. Atmos. Sci.*, **37,** 131–147.

Hansen, J., and S. Lebedeff, 1988: Global surface air temperatures: Update through 1987. *Geophys. Res. Lett.*, **15,** 323–326.

——, G. Russell, D. Rind, P. Stone, A. Lacis, S. Lebedeff, R. Ruedy, and L. Travis, 1983: Efficient three-dimensional global models for climate studies: Models I and II. *Mon. Wea. Rev.*, **111,** 609–662.

——, I. Fung, A. Lacis, D. Rind, S. Lebedeff, R. Ruedy, G. Russell, and P. Stone, 1988: Global climate changes as forecast by Goddard Institute for Space Studies three-dimensional model. *J. Geophys. Res.*, **93,** 9341–9364.

Hasselmann, K., 1976: Stochastic climate models. Part I. Theory. *Tellus,* **6,** 473–485.

Hess, P. G., D. S. Battisti, and P. J. Rasch, 1993: Maintenance of the intertropical convergence zones and the large-scale tropical circulation on a water-covered earth. *J. Atmos. Sci.*, **50,** 691–713.

James, I. N., and P. M. James, 1989: Ultra-low-frequency variability in a simple atmospheric circulation model. *Nature,* **342,** 53–55.

Jenkins, G. M., and D. G. Watts, 1968: *Spectral Analysis and Its Applications.* Holden-Day, 525 pp.

Liu, W. T., and C. Gautier, 1990: Thermal forcing on the tropical Pacific from satellite data. *J. Geophys. Res.*, **95,** 13 209–13 217.

MacVean, M. K., and P. J. Mason, 1990: Cloud-top entrainment instability through small-scale mixing and its parameterization in numerical models. *J. Atmos. Sci.*, **47,** 1012–1030.

Manabe, S., and R. J. Stouffer, 1988: Two stable equilibria of a coupled ocean–atmosphere model. *J. Climate,* **1,** 841–866.

Mehta, V. M., 1992: Meridionally propagating interannual-to-interdecadal variability in a linear ocean–atmosphere model. *J. Climate,* **5,** 330–342.

Miller, J. R., G. L. Russell, and L.-C. Tsang, 1983: Annual oceanic heat transports computed from an atmospheric model. *Dyn. Atmos. Oceans,* **7,** 95–109.

Miller, R. L., and A. D. Del Genio, 1994: Cloud feedbacks and interannual climate variability. *Proc. Sixth Conf. on Climate Variations,* Nashville, TN, Amer. Meteor. Soc., 50–53.

Press, W. H., S. A. Teukolsky, W. T. Vettering, and B. P. Flannery, 1992: *Numerical Recipes in Fortran.* 2d ed. Cambridge University Press, 963 pp.

Randall, D. A., 1980: Conditional instability of the first kind upside-down. *J. Atmos. Sci.*, **37,** 125–130.

Sausen, R., K. Barthel, and K. Hasselmann, 1988: Coupled ocean–atmosphere models with flux correction. *Climate Dyn.*, **2,** 145–163.

Schlesinger, M. E., and J. F. B. Mitchell, 1987: Climate model simulations of the equilibrium climatic response to increased CO_2. *Rev. Geophys.*, **25,** 760–798.

Siems, S. T., C. S. Bretherton, M. B. Baker, S. Shy, and R. E. Briedenthal, 1990: Buoyancy reversal and cloud-top entrainment instability. *Quart. J. Roy. Meteor. Soc.*, **116,** 705–739.

Slingo, J. M., 1980: A cloud parameterization scheme derived from GATE data for use with a numerical model. *Quart. J. Roy. Meteor. Soc.*, **106,** 747–770.

Weaver, A. J., and E. S. Sarachik, 1991: Evidence for decadal variability in an ocean general circulation model: An advective mechanism. *Atmos.-Ocean,* **29,** 197–231.

——, and T. M. C. Hughes, 1993: Stability and variability of the thermohaline circulation and its link to climate. *Trends Phys. Oceanogr., Council of Scientific Research Integration, Research Trends Series, Trivandrum, India,* **1,** 15–70.

Wigley, T. M. L., and S. C. B. Raper, 1990: Natural variability of the climate system and detection of the greenhouse effect. *Nature,* **344,** 324–327.